Optimization of Lateral Position of Autonomous Trucks

by
Osman Erman Gungor
Ruifeng She
Imad L. Al-Qadi
Yanfeng Ouyang
University of Illinois at Urbana—Champaign

DISCLAIMER

Suggested APA Format Citation:

Gungor, O. E., She, R., Al-Qadi, I. L., & Ouyang, Y. (2018). *Optimization of lateral position of autonomous trucks* (Report No. ICT-20-009). Illinois Center for Transportation. https://doi.org/10.36501/0197-9191/20-009

Contacts:

Osman Erman Gungor
University of Illinois at Urbana–Champaign
Illinois Center for Transportation
1611 Titan Drive
Rantoul, IL 61866
gungor2@illinois.edu
(217) 300-1488
https://ict.illinois.edu

CCAT
University of Michigan Transportation Research Institute
2901 Baxter Road
Ann Arbor, MI 48152
uumtri-ccat@umich.edu
(734) 763-2498
www.ccat.umtri.umich.edu

TECHNICAL REPORT DOCUMENTATION PAGE

1. Report No. ICT-20-009	2. Government Accession No. N/A	3. Recipient's Catalog No. N/A	
4. Title and Subtitle Optimization of Lateral Position of Autonomous Trucks		**5. Report Date** November 2018	
		6. Performing Organization Code N/A	
7. Authors Osman Erman Gungor, Ruifeng She, Imad L. Al-Qadi, and Yanfeng Ouyang		**8. Performing Organization Report No.** ICT-20-009 UILU-ENG-2020-2009	
9. Performing Organization Name and Address Illinois Center for Transportation Department of Civil and Environmental Engineering University of Illinois at Urbana–Champaign 205 North Mathews Avenue, MC-250 Urbana, IL 61801		**10. Work Unit No.** N/A	
		11. Contract or Grant No. Grant No. 69A3551747105	
12. Sponsoring Agency Name and Address Center for Connected and Automated Transportation University of Michigan Transportation Research Institute 2901 Baxter Road Ann Arbor, MI 48152		**13. Type of Report and Period Covered** N/A	
		14. Sponsoring Agency Code Center for Connected and Automated Transportation	

16. Abstract

The introduction of autonomous and connected trucks (ACTs) is expected to result in drastic changes in operational characteristics of freight shipments, which may in turn have significant impacts on efficiency, safety, energy consumption, and infrastructure durability. One such change is the formation of truck platoons. Truck platoons will become more feasible and practical with the intelligent technologies existing in ACTs that enable the connection among vehicles and between vehicles and infrastructure. Some reported and expected benefits of platooning are reducing congestion, braking/accelerating, and improving fuel efficiency. Yet, such platooning operations may accelerate the damage accumulation within pavement structures due to the trucks' similar lateral positions (i.e., wheel wander) within the lane. Therefore, this study develops a platooning-control strategy for a fleet of ACTs such that trucks' lateral shifts within a lane can be explicitly optimized to minimize damage to the pavement, thus significantly reducing maintenance and rehabilitation costs. The efficacy of the proposed strategy was demonstrated through a case study. The results showed that the cost of platooning can be reduced by approximately $0.5 million/mi, depending on the platoon size, pavement thickness, and traffic.

17. Key Words Platooning, Optimization, Autonomous and Connected Trucks	**18. Distribution Statement** No restrictions. This document is available through the National Technical Information Service, Springfield, VA 22161.		
19. Security Classif. (of this report) Unclassified	**20. Security Classif. (of this page)** Unclassified	**21. No. of Pages** 26	**22. Price** N/A

Form DOT F 1700.7 (8-72)   **Reproduction of completed page authorized**

ACKNOWLEDGMENT, DISCLAIMER, MANUFACTURERS' NAMES

TABLE OF CONTENTS

LIST OF FIGURES

LIST OF TABLES

CHAPTER 1: INTRODUCTION

OVERVIEW

The transportation sector is the second largest element of the global energy sector, with an oil demand of 52 million barrels (mb) per day. Furthermore, it has had the fastest growing oil demand among all sectors since 2000, with a 1.9% annual growth rate. Within the transportation sector, road freight is one of the key contributors to oil demand. By 2016, road-freight vehicles consumed 17 mb of oil per day, which is just 6 mb/d less than that consumed by passenger vehicles. Moreover, the demand growth in road freight outpaced that of all other sectors; and it is expected to increase by a factor of 2.4 by 2050 (IEA, 2017).

To reduce this high and growing oil demand, many attempts have been made in the road-freight industry to improve trucks' fuel efficiency, such as the introduction of wide-base tires (Gungor et al., 2016), aerodynamically reinforced truck designs (Smith et al., 2012), or optimizing truck routing (Suzuki, 2011). One idea to increase fuel efficiency of road freight is to place trucks after one another within a close distance by using autonomous and connected truck (ACT) technology. This group, or convoy, of trucks is called a *platoon*. While the safe distance for human-driven trucks is 165 ft in Europe and 200 ft in the United States, enabling communication technologies embedded in ACTs can reduce this distance to 10 ft in a platoon (Browand et al., 2004).

The main advantage of placing trucks at a close distance is reducing the overall aerodynamic drag on them. Most of the aerodynamic drag (70% to 90%) is caused by the pressure difference between the front (high-pressure zone) and rear (low-pressure zone) of a truck, which is called the pressure drag (Gaudet, 2014). In a platoon, the pressure drag on trailing trucks decreases because the trucks in front block the air, which lowers the pressure in the frontal zone (i.e., high-pressure zone). For leading trucks, aerodynamic drag decreases because the trailing truck compresses the turbulent flow that increases the pressure in the low-pressure zone. Consequently, this reduction in aerodynamic drag leads to decreased fuel consumption and increased fuel efficiency.

Numerous studies have tried to quantify the reduction in fuel consumption due to platooning. The first study was conducted in the mid-1990s (Tsugawa et al., 2016) within the scope of a European Union (EU) project called "Chauffeur" (Bonnet & Fritz, 2000). The platoon tested was composed of two partially loaded, tandem trucks travelling at a speed of 80 km/h. This study stated that while the trailing truck consumed 20% less fuel in the platooning truck for 10 m of intervehicle spacing, this reduction decreased to 6% for the lead truck. In 2004, two identical trucks with varying spacing (i.e., 3, 4, 6, 8, and 10 m) were tested on an unused road by the California Partners for Advanced Transportation Technology (PATH) program (Browand et al., 2004). Two speeds were selected, 50 and 80 km/h. Later, the fuel savings were averaged over the different intervehicle spacings and speeds. The resultant average fuel savings were 10% and 6% for the trailing and lead trucks, respectively. In 2011, three trucks were tested in the PATH program (Lu & Shladover, 2011). A 6% increase in fuel savings on average was observed, as compared to two-truck platooning. Between 2005 and 2009, a series of field platooning tests consisting of four heavy trucks was conducted in Aachen University under the project named "KONVOI," which also demonstrated the viability and efficiency of truck

platooning. Other key studies about truck platooning and fuel efficiency were Energy ITS in Japan (Tsugawa et al., 2011; Tsugawa 2014); SARTRE (Robinson et al., 2010); COMPANION (Eiler et al., 2015); as well as ETPC for the EU (Jacob & Arbeit, n.d.) and in the United States (Lammert et al., 2014; Alam et al., 2015; Humphreys et al., 2016). In addition to increasing fuel efficiency, truck platoons are expected to reduce congestion and breaking/accelerating as well as improve roadway safety.

PROBLEM STATEMENT AND OBJECTIVE

The main motivation behind the development of truck platooning is the reduction of fuel consumption and emissions that is obtained by positioning the trucks one after another to reduce aerodynamic drag. Most of the aerodynamic drag (70% to 90%) is caused by the pressure difference between the front (high-pressure zone) and the rear (low-pressure zone) of a truck, known as the pressure drag (Gaudet, 2014). In a platoon, the pressure drag on trailing trucks decreases because the trucks in front of them block the air, which lowers the pressure in the frontal zone (i.e., high-pressure zone). For leading trucks, aerodynamic drag decreases because the trailing truck compresses the turbulent flow, which increases the pressure in the low-pressure zone.

However, such platooning operations may accelerate damage accumulation within pavement structures because the lateral position of successive ACTs within a lane is expected to be similar (i.e., channelized traffic), while it is more scattered for human-driven trucks. Therefore, this study develops a platooning-control strategy for a fleet of ACTs such that trucks' lateral shifts within a lane can be explicitly optimized to minimize pavement damage, hence, significantly reducing maintenance and rehabilitation (M&R) costs.

The result of the optimization process is depicted in Figure 1-B. This figure can be interpreted as an "optimized" pattern for a platoon of a given number of trucks. In other words, this study determines the optimum configuration of lateral position of trucks in a platoon (or a platoon skeleton) for a specific number of trucks. It is assumed that a configuration (or pattern) such as this can be initiated and sustained within a platoon through vehicle-to-vehicle (V2V) communication as the trucks travel.

METHODOLOGY

To accomplish the objective of this study (i.e., optimizing the lateral position of trucks in a platoon), one should simulate the impact of manipulating the lateral position of trucks on pavement-damage accumulation and truck aerodynamics. Thereby, costs (i.e., R&M cost and fuel cost) can be minimized over the truck configuration. The framework of the study is given in Figure 2. The framework is built on three elements: pavement design and analysis, truck aerodynamics modeling, and optimization.
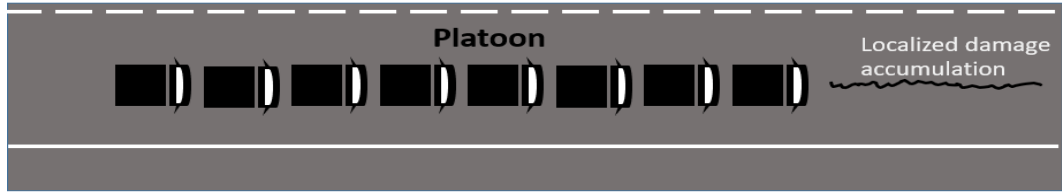
(A) Do-nothing scenario: There is no lateral offset.
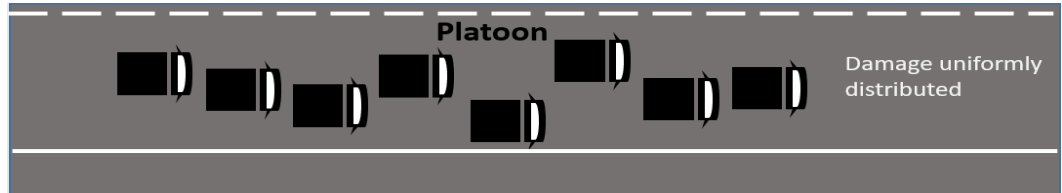
(B) Optimized scenario: An optimized pattern is developed for a given number of trucks.

Figure 1. Photo. Optimization of lateral position of ACTs in a platoon using vehicle-to-vehicle (V2V) communication.
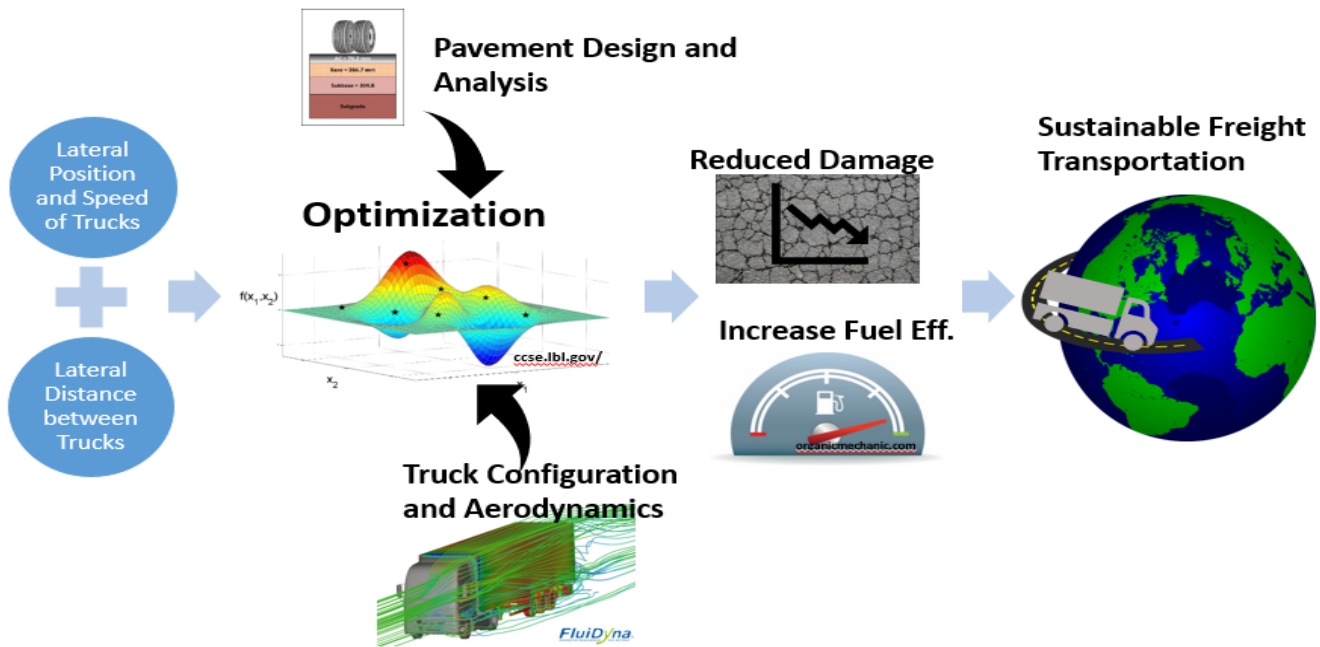
Figure 2. Photo. Illustration of the methodology.

CHAPTER 2: PAVEMENT DESIGN AND ANALYSIS

To the best of the authors' knowledge, no pavement-design guideline in the literature can take the lateral position of trucks as an explicit input. Therefore, there is a need to develop a new pavement-design guideline that can simulate the impact of any arbitrary lateral positioning of trucks on pavement-damage accumulation so that the optimization problem can be solved.

To fill the gap in the literature, the authors developed a pavement-design framework that reinforces the state-of-the-practice pavement-design guideline called MEPDG (NCHRP, 2004), using techniques from statistics and applied mathematics to enable explicit consideration of truck's lateral position. This framework has been explained in detail elsewhere (Gungor et al., 2018). A summary of the framework developed is presented below (Figure 3).

PAVEMENT RESPONSES

This step of the framework developed corresponds to the mechanistic part of MEPDG. In this step, the critical pavement responses are computed under a tire load with given material properties and pavement structure. This study uses three-dimensional (3D) advanced-pavement finite-element (FE) models developed and continuously improved by Al-Qadi and his coworkers over more than 15 years (Elsefi et al., 2006; Yoo & Al-Qadi, 2007; Wang & Al-Qadi, 2010; Al-Qadi & Wang 2012; Al-Qadi et al., 2015; Hernandez & Al-Qadi, 2016; Gungor et al., 2016a, 2016b, 2017; Castillo & Al-Qadi, 2018). FE models bring many advantages, as compared to conventional approaches to pavement structural analysis (e.g., layered elastic theory), such as simulation of asphalt concrete (AC) as viscoelastic and unbound layers as nonlinear stress-dependent material, and incorporation of measured 3D contact stresses, along with the true tire footprint.
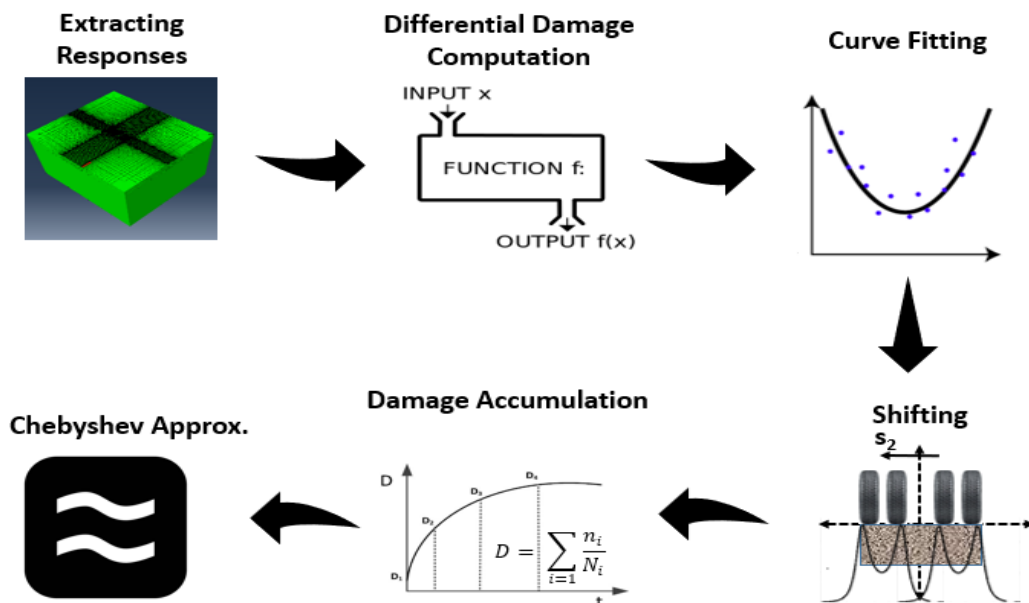
Figure 3. Photo. Pavement-design framework.

DIFFERENTIAL DAMAGE COMPUTATION

The damage-prediction framework developed by MEPDG consists of two steps. The initial step answers the question of how much damage occurs when a strain is applied for N times. In other words, the strains are transformed into damage that occurs after a number of load repetitions. This transformation is done by using transfer functions. Herein, this step is referred to as a *differential damage computation*. The outcomes of this step are rutting at the mid-depth of each layer and a fatigue-damage index for fatigue-crack prediction.

Whenever an input that alters the value of the computed strain (e.g., different modulus due to temperate changes or different axle load) changes, the differential damage-computation step is repeated. After each repetition, the outcomes are fed into damage-accumulation equations to predict the final damage. These accumulation equations are explained later in the report. The following sections explain the computation of the parameters in the differential damage computation.

Damage Index

The formula for the damage index is given in Figure 4.

$$DI = \frac{n}{\vec{N}}$$

Figure 4. Equation. Damage index.

where n = number of load repetitions, derived from traffic data; $\vec{N}$ = the vector of the computed allowable number of repetitions, using transfer functions at each transverse location. The current version of the formula used for calculating the number of repetitions to failure is given in Figure 5.

$$\vec{N} = k_{f1} C C_H B_{f1} \left(\frac{1}{\vec{\varepsilon_t}}\right)^{k_{f2}\beta_{f2}} \left(\frac{1}{E}\right)^{k_{f3}\beta_{f3}}$$

Figure 5. Equation. Number of repetitions to failure.

where $\vec{\varepsilon_t}$ = vector of extracted tensile strains at the bottom of AC (asphalt concrete) for each transverse location; E = dynamic modulus of the hot-mix asphalt (HMA) layer (psi); k_{f1}, k_{f2}, k_{f3} = global field-calibration factors: 0.007566, 3.9492, and 1.281, respectively; β_{f1}, β_{f2}, β_{f3} = local calibration factors that are set to 1.0 by default. In addition:

$$C = 10^M$$

$$M = 4.84 \left(\frac{V_{be}}{V_a + V_{be}} - 0.69\right)$$

Figure 6. Equation. Some material constants needed for number of repetitions to failure.

where V_{be} = efffective asphalt content by volume (%); V_a = percent air voids in the HMA mixture; and C_H = thickness-correction term, depending on the type of cracking (Figure 7 or Figure 8).

For bottom-up fatigue cracking:

$$C_H = \frac{1}{0.000398 + \frac{0.003602}{1 + e^{11.02 - 3.49H_{HMA}}}}$$

Figure 7. Equation. Thickness correction term for bottom-up cracking.

For top-down cracking:

$$C_H = \frac{1}{0.01 + \frac{12}{1 + e^{15.676 - 2.8186H_{HMA}}}}$$

Figure 8. Equation. Thickness correction term for top-down cracking.

Asphalt Concrete (AC) Rutting

The current version of the formula used for calculating the rutting within AC is given in Figure 9.

$$\vec{\delta} = h_{sub}\beta_{r1}k_z\vec{\varepsilon_v}10^{k_{31}}n^{k_{r2}\beta_{r2}}T^{k_{r3}\beta_{r3}}$$

Figure 9. Equation. Rutting equation for asphalt concrete.

where h_{sub} = thickness of sub-layer (Algorithm 1); $\vec{\delta}$ = the vector of predicted rutting at the mid-depth of each sub-layer of the AC layer at each critical transverse location; $\vec{\varepsilon_v}$ = the vector of vertical compressive strain at the mid-depth of each sub-layer at each critical transverse location; n = Repetition number of the load that developed $\varepsilon_{r(AC)}$ at given climatic conditions; T = temperature at the mid-depth of each sub-layer (°F); k_{r1}, k_{r2}, k_{r3} = global field-calibration factors: −0.3512, 0.4791 and 1.5606, respectively; β_{r1}, β_{r2}, β_{r3} = local calibration factors that are set to 1.0 by default. In addition:

$$k_z = (C_1 + C_2D)0.328196^D$$

$$C_1 = -0.1039\ h_{AC}^2 + 2.4868h_{AC} - 17.342$$

$$C_2 = 0.0172h_{AC}^2 - 1.7331h_{AC} + 27.428$$

Figure 10. Equation. Some constants needed for rutting calculation.

where D = mid-depth of the sub-layer from the surface (in.) and h_{AC} = total AC thickness.

Rutting in Unbound Layers

The current version of the formula used for calculating the rutting within unbound materials is given in Figure 11.

$$\vec{\delta} = h_{sub}\, \beta_{r1} k_{r1} \left(\frac{\varepsilon_0}{\varepsilon_r}\right) e^{-\left(\frac{\rho}{n}\right)^{\beta}} \vec{\varepsilon_v}$$

Figure 11. Equation. Rutting in unbound layers.

where k_{r1} = global field-calibration factors: 2.03 for granular materials and 1.35 for fine-grained materials; and β_{r1} = local calibration factor, set to 1 by default. In addition:

$$\beta = 10^{0.6119 - 0.017638\, W_c}$$

$$\left(\frac{\varepsilon_0}{\varepsilon_r}\right) = \frac{e^{(\rho^{\beta})}a_1 + e^{\left(\frac{\rho}{10^9}\right)^{\beta}} a_9}{2}$$

$$\rho = 10^9 \left(\frac{C_0}{1 - (10^9)^{\beta}}\right)^{\frac{1}{\beta}}$$

$$W_c = 51.712 \left[\left(\frac{E}{2555}\right)^{\frac{1}{0.64}}\right]^{-0.3586 * GWT^{0.1192}}$$

$$C_o = \ln\left(\frac{a_1}{a_9}\right)$$

Figure 12. Equation. Some material constants required for rutting calculations.

CURVE FITTING

In this step, the responses and damages computed at discrete points are converted to a continuous function by curve fitting using least-squares regression. The target variable for curve fitting differs, depending on the type of damage parameter. For fatigue cracking, the curve is fitted to the final computed damage parameter, i.e., the vector of DI (Figure 4). By contrast, for rutting computation, the curve is fitted directly to the response vector. The formula for curve fitting is given in Figure 13.

$$f(x) = \sum_{i=0}^{n} \alpha_i \phi(x)^i$$

Figure 13. Equation. Curve fitting equation.

where y = response or damage vector; x = continuous axis that represents the cross section of a wheel path; $f(x)$ = fitted curve function. In addition:

$$\phi(x) = e^{-\left(\frac{x'}{w_h \gamma}\right)^2}$$

Figure 14. Equation. Nonlinear transformation.

where x' = normalized axis by wheel-path width; w_h = wheel-path width; γ = smoothing parameter; and α_i = regression coefficient that is computed using least-squares regression.

SHIFTING

The framework developed interprets wheel wander as the shift of the function obtained at the curve-fitting step. In the framework, two types of shifts may be considered: (1) deterministic, which can be interpreted as ACTs with very advanced technology not exhibiting any random lateral movement as they travel, and (2) probabilistic, which can incorporate randomness on the lateral position of the vehicles (i.e., wheel wander) at any level. The mathematical formulation for the aforementioned shifting can be defined as mapping *x* to *x-s-t*, where *s* stands for a random variable for wheel wandering and *t* stands for deterministic shifting. The formulation for the shifted function is given in Figure 15.

$$f(x,t,s) = \sum_{i=0}^{n} \alpha_i e^{-i\left(\frac{x-t-s}{w_h \gamma}\right)^2}$$

Figure 15. Equation. Applying deterministic and probabilistic shifting.

where *s* = random variable that follows a truncated normal distribution.

In Figure 15, $f(x,s,t)$ has become a random function due to the variable s. To compute the resultant damage profile, the expectation of this function (i.e., $E[f(x,s,t)]$) should be calculated. For only deterministic shifting (where s equals zero and t equals some real number), the calculation of expectation is straightforward; and it is done by substituting the value of t into Figure 15.

DAMAGE ACCUMULATION

Rutting Accumulation

MEPDG uses a nonlinear strain-hardening approach to simulate the rutting accumulation after each discrete step. This approach starts with the computation of equivalent repetition, which is defined as the number of repetitions that would cause the previously accumulated rutting using current computed vertical strain. Figure 16 formulates this statement where only the unknown variable is n_{eq}.

$$\overline{\delta_{acc}(x)} = \delta(T_i, \overline{\varepsilon_{vi}(x)}, n_{eq}(x), \vec{C})$$

Figure 16. Equation. Rutting accumulation after applying shifting.

where $\overline{\delta_{acc}(x)}$ = accumulated rutting profile until the ith step at each transverse location, considering wheel wander; $\overline{\varepsilon_{vi}(x)}$ = fitted function to extracted compressive strains at the critical locations at the ith step after applying shifting; $n_{eq}(x)$ = profile of equivalent number of repetitions, which amounts to the solution of Figure 16; and $\delta(T_i, \overline{\varepsilon_{vi}(x)}, n_{eq}(x))$ = predicted rutting profile at each transverse location, which can be computed using empirical functions given in Figures 9 and 11, depending on the material type under the loading and climatic conditions (e.g., T_i) at i^{th} step.

After solving Figure 13 for $n_{eq}(x)$, it is added to the number of repetitions of the current strain. Finally, the total number of repetitions, along with the current strain, is plugged in rutting empirical functions to compute the accumulated rutting (Figure 17).

$$\overline{\delta_i(x)} = \delta(T_i, \overline{\varepsilon_{vi}(x)}, n_{eq}(x) + n_i, \vec{C})$$

Figure 17. Equation. Accumulated rutting at step i.

where $\overline{\delta_i(x)}$ = accumulated rutting profile at the ith step; and n_i = number of repetitions at the ith step.

Finally, total rutting is computed by summing the accumulated rutting at each sub-layer (Figure 18).

$$RD_i(x) = \sum_{j=1}^{M} \overline{\delta_{ji}(x)}$$

Figure 18. Equation. Total rutting, summation of rutting from each layer.

where RD_i = total accumulated rutting profile at the ith step; and M = number of sub-layers.

Fatigue Cracking

Damage accumulation for fatigue cracking is simulated using Miner's Law, given in Figure 19.

$$D_i(x) = \sum_{k=1}^{i} DI_k(x)$$

Figure 19. Equation. Accumulated damage index at step i.

where $D_i(x)$ = accumulated fatigue-damage profile at the ith step.

Afterwards, using the transfer functions given in Figure 20 and Figure 21, resultant bottom-up and top-down fatigue cracking are computed.

$$FC_i^{bottom}(x) = \left(\frac{1}{60}\right)\left(\frac{C_4}{1 + e^{C_1 C_2^* + C_2 C_2^* log(D(x)*100)}}\right)$$

Figure 20. Equation. Bottom-up cracking.

where $FC_i^{bottom}(x)$ = percent of alligator-cracking profile that initiates at the bottom of the HMA layers at the ith step; C_1, C_2, C_4 = calibration factors that equal 1, 1, and 6, respectively; $C_1^* = -C_2^*$; $C_2^* = -2.40874 - 39.748(1 + h_{ac})^{-2.856}$. In addition:

$$FC_i^{top}(x) = 10.56 \left(\frac{C_4}{1 + e^{C_1 - C_2 log(D(x)*100)}} \right)$$

Figure 21. Equation. Top-down cracking.

where $FC_i^{top}(x)$ = length of longitudinal cracks profile that initiates at the top of the HMA layer (ft/mi) at the ith ste; and C_1, C_2, C_4 = calibration factors that equal 7, 3.5, and 1, respectively.

International Roughness Index (IRI)

After the accumulated damage is computed, IRI progression is simulated using Figure 22.

$$IRI(x) = IRI_0 + C_1(RD) + C_2 FC_{total} + C_3 TC + C_4 SF$$

Figure 22. Equation. IRI.

where IRI_0 = initial IRI after construction in./mi; RD = accumulated rutting depth from all layers (in.); FC_{total} = total amount of fatigue cracking, summation of bottom-up and top-down cracking; TC = thermal cracking. It should be noted that because thermal cracking is not a load-related distress, it is not studied in this report. The amount of accumulated thermal cracking can be computed by running commercial AASHTOWare software and integrated to the framework; C_1, C_2, C_3, C_4 = calibration factors, which equal 40, 0.4, 0.008, and 0.015, respectively; and SF = site factor.

CHEBYSHEV APPROXIMATION TO ACCUMULATED DAMAGE

Accumulated damage equations become too complex to store and compute after a couple of accumulation steps due to the use of continuous functions. Therefore, damage accumulation equations should be simplified using function approximation. The framework developed uses Chebyshev approximation, which can globally approximate any bounded function with a desired level of accuracy (Figure 23).

$$g(y) \approx \sum_{k=0}^{p} h_k R_k(y)$$

Figure 23. Equation. Chebyshev approximation.

where $g(y)$ = the function to be approximated, i.e., it is the accumulated damage at the ith step; $R_k(y)$ = Chebyshev polynomials (Figure 24); and h_k = Chebyshev coefficients.

$$R_p(y) = cos(pcos^{-1}(y)) = y^p \sum_{k=0}^{*\frac{p}{2}} P_{2k}(1 - y^{-2})^k$$

Figure 24. Equation. Chebyshev polynomials.

where $R_p(y)$ = pth degree Chebyshev polynomial; and y = real numbers between −1 and 1.

CHAPTER 3: TRUCK AERODYNAMICS

In truck platooning, the total drag force incurred on both trucks is reduced by having a small inter-vehicle spacing such that the head of a truck is under the influence of the wake of the preceding one. This phenomenon has been observed in wind tunnel tests (Zabat et al., 1995). The drag reduction is affected by the relative position of the adjacent vehicles and diminishes as the vehicles are placed further apart, or completely misaligned. Limited test results are available in the literature for freight trucks of large platoon sizes with consideration of lateral misalignment. In this study, the pair-wise drag reduction as a function of relative position (lateral and longitudinal) is simulated using Ansys Fluent, a computational fluid dynamics (CFD) solver, and an interpolation model is designed to estimate the total fuel savings for the entire platoon.

The drag force is simulated over two modified Ahmed bodies (Liu & Moser, 2003), with additional features, such as curved edges and inclined frontal surface to capture the common aerodynamic design on modern freight trucks. Accessories such as side mirrors and tires are omitted as they do not have significant impact on the incurred drag force. According to the Fluent 14.0 theoretical guide (Ansys, 2011), the most suitable governing equations for incompressible turbulent-flow problems is the Reynolds-averaged Navier-Stokes equations (RANS). RANS accurately examine drag force under the influence of a wake with computational efficiency. The turbulence model used is the realizable k-ϵ model (RKE), where k is the turbulent kinetic energy and ϵ is the turbulent dissipation rate. RKE handles turbulent-dissipation features in flows with strong curvature and rotation (Lanfrit 2005), as in the wake region encountered by the trailing truck. The disadvantage of RKE lies in its inability to capture re-lamination (Spalart, 1997). However, according to Hinterberger et al. (2004), this property does not significantly impact the result because re-lamination completes around 45 to 60 m behind the truck body. At this distance, the economic benefit of platooning diminishes, and it is not of interest in this study, as the optimal inter-vehicle separation is expected to be within 3 to 25 m. For near-wall treatment, the nonequilibrium wall functions were used for better handling of separated flows above a moving-wall boundary condition. The solution control settings referred to Humphreys (2017) and the ANSYS Fluent 14.0 User's Guide (2011), which were also adopted by other researchers such as Van Leeuwen (2009). The simulation yields the drag coefficients for both the leading and trailing truck, which serves as the input to the interpolation model for the total fuel consumption of the platoon.

MESH DEVELOPMENT

ANSYS Meshing enforces mesh quality with two major criteria: maximum face size and skewness. Adaptive meshing is used to refine oversized or ill-shaped elements until the criteria are met. In cases where adaptive meshing is not able to provide satisfactory results, such as around sharp edges or angles, or where higher turbulence is anticipated, the mesh is refined manually.

Three major methods are used to improve mesh quality. First, inflation layers are defined on the surfaces of interest, e.g., test body and road surfaces. This approach is widely used in CFD to accommodate large velocity gradients within boundary layers where shear stresses are developed upon contact between fluid and solid surfaces. Finer meshes are required near these boundaries to

capture the drastic change in the velocity profile. In ANSYS Meshing, inflation layers define surfaces with a series of thin prisms that grow outward as a smooth transition to tetrahedral elements. Figure 25 shows the local meshing implementing inflation layers. Second, refinement boxes can be defined in regions where wakes are expected to form. These regions are located behind the truck bodies, where the flow is most turbulent under the separation–convergence motion. Figure 26 shows the mesh after adding a refinement box between the two truck bodies. The mesh maximum face size, defined as the length of the longest edge of an element, is selected to be much smaller within these boxes to achieve higher accuracy. The third approach is to manually improve mesh quality at low-quality elements by adding partitions or moving nodes. ANSYS Meshing provides full control to edit elements directly. This approach can be labor-intensive and is generally used as a last resort when only a small number of elements needs to be treated. Around 1.2 million to 1.5 million elements are generated in each simulation.
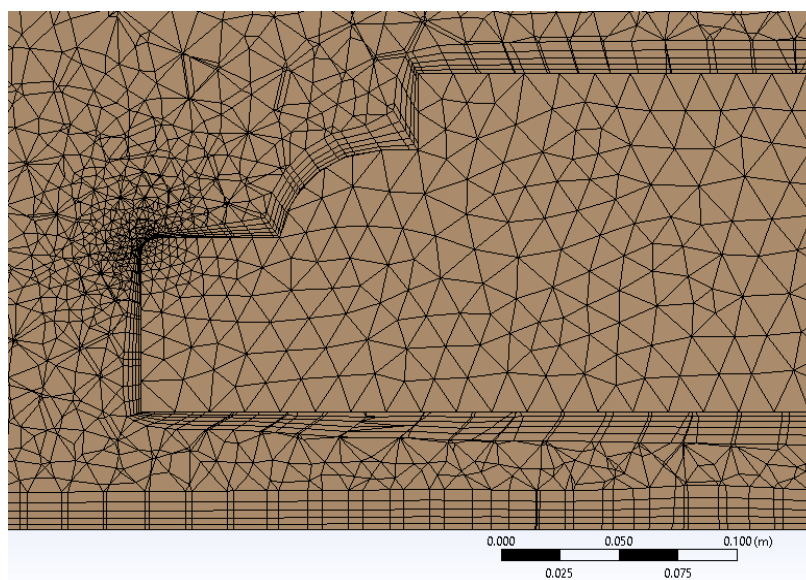
Figure 25. Photo. Illustration of inflation layers implemented at boundaries.
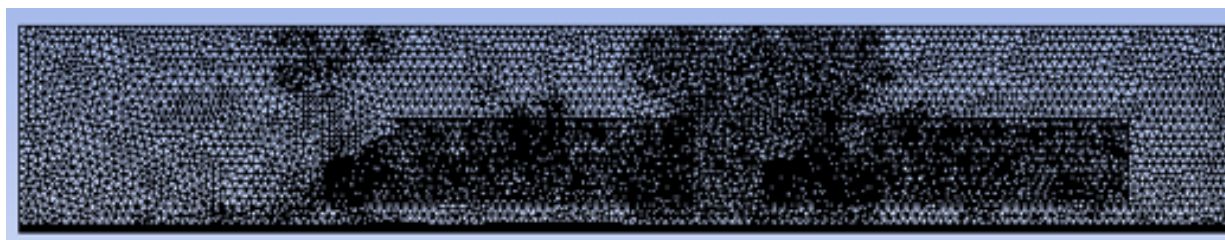
Figure 26. Photo. Illustration of refined box implemented at wake region.

SIMULATION RESULTS

The CFD simulation results are presented in Figure 27, which shows the static pressure contour on the truck bodies with 9 m separation and 0.3 m lateral offset, where the gauge pressure is 0 Pa at the outlet. One can observe that the trailing truck suffers significantly less pressure drag because of the

platooning effect. To quantify the reduction in pressure drag in platoons, the concept of drag ratio is introduced. This ratio is computed by dividing the drag coefficient of trucks in a platoon to that of isolated truck (i.e., without platooning effect). In other words, drag ratios are normalized drag coefficients of trucks in a platoon with respect to that of an isolated truck. Figure 30 shows the simulated drag ratio over various separation and lateral offset. As seen, the drag reduction is most significant when vehicles are closely placed and aligned and diminishes as they deviate, which agrees with the wind tunnel test by Zabat et al. (1995). Additionally, this contour was used as an interpolation function in this study to calculate the drag ratios for arbitrary configuration of trucks in a platoon (i.e., for various truck separations and lateral offsets).
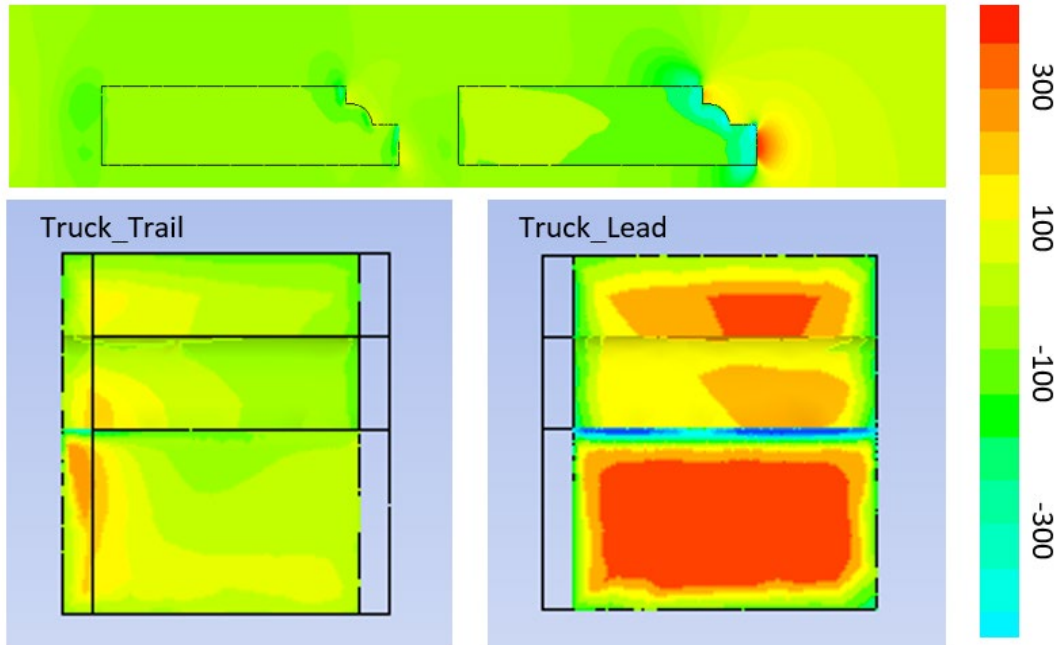
Figure 27. Photo. Pressure contour on center plane; frontal surface of trailing truck; frontal surface of leading truck (Units in Pa).

After obtaining drag coefficients, the fuel cost due to aerodynamics can be calculated by Figure 28.

$$cost_{drag}\left(\frac{\$}{VMT}\right) = c_a \frac{1}{2}\rho A C_{D,\infty} v^2 \sum_{i=1}^{N} R_i\,(s, \varDelta x)$$

Figure 28. Equation. Fuel cost due to aerodynamics.

Figure 28 computes the monetary value per vehicle miles traveled (VMT). In Figure 28, ρ is the air density 1.225 kg/m^3, v is the cruising velocity 26.8 m/s, A is the cross-sectional area of the simulated body 9.49 m^2, c_a is a unit converting factor 2.743e-8 L/J based on an engine efficiency of 40% and a typical diesel price of \$0.74 per L and $C_{D,\infty}$ is the drag coefficient of an isolated trucks computed from developed CFD simulations. The only unknown left in Figure 28 is $R_i(s, \varDelta x)$, which is computed by Equation 6.

$$R_i = R_L(s) - \sum_{\substack{j=1 \\ j \neq i}}^{i} \frac{R_L(s) - \widehat{R_{j+1}}(\Delta_{j-i}, s)}{R_L(s) - R_T(s)} \Delta R_j$$

Figure 29. Equation. Drag Coefficient.

where

$R_L(s)$ and $R_T(s)$ = field drag coefficients for leading and trailing trucks for two-trucks platoon given inter-vehicle spacing (Zabat et al., 1995);

$\widehat{R_{j+1}}(\Delta_j, s)$ = drag coefficient of $(j+1)^{th}$ truck obtained from CFD simulations (Figure 6);

Δ_{j-i} = lateral distance between j^{th} and i^{th} trucks;

s = inter-vehicle distance between trucks in a platoon;

ΔR_j = drag coefficient difference between j^{th} and $(j+1)^{th}$ computed from Zabat et al. (1995); it stays the same after the fourth truck.

Figure 30. Chart. Surface plot of drag ratio for the trailing vehicle.

CHAPTER 4: OPTIMIZATION

There is a trade-off between fuel cost due to reduced aerodynamic drag in a platoon and pavement life cycle cost. While perfectly aligned trucks (i.e., all the trucks have the same lateral position) and small inter-vehicle distance in a platoon decrease the fuel consumption of trucks, such platooning application may accelerate the damage accumulation within pavement structure, which, in turn, will increase the pavement life cycle cost that is the summation of agency cost and user 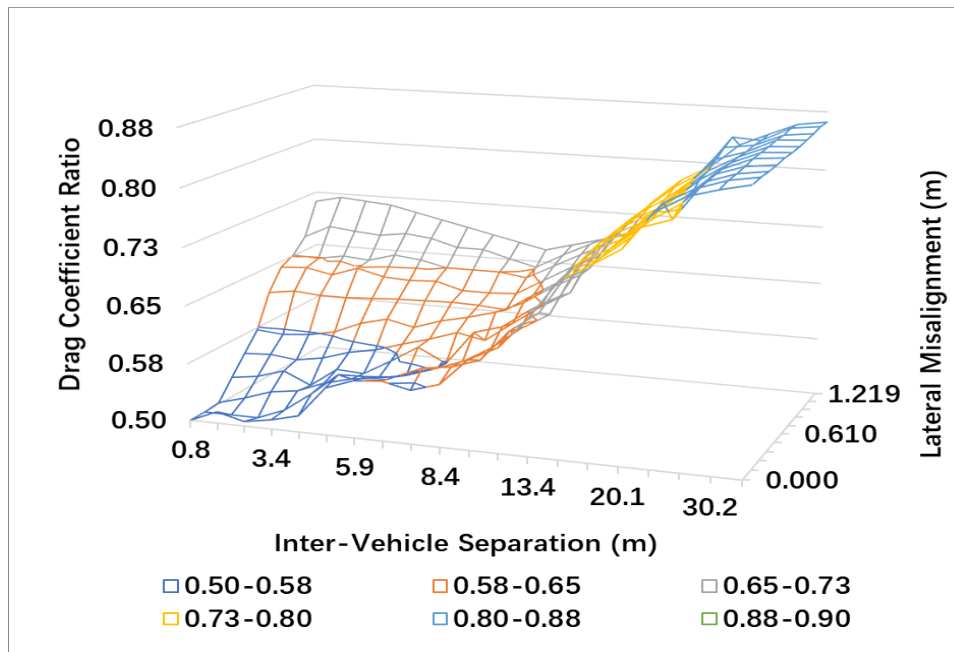cost. This study aims to minimize the summation of these two costs (i.e., overall cost) by optimizing the trade-off between them. The computation of fuel cost due to aerodynamic drag reduction is given in Figure 28. In the remainder of this section, the computation of pavement life cycle cost is introduced.

The pavement life cycle cost has two main parts: agency cost and user cost. Agency cost includes the costs of rehabilitation, maintenance, and construction activities conducted by state transportation agencies. In this study, the elements of agency costs that are not affected by the traffic loads such as initial construction cost or the cost of regular maintenance activities are omitted. Therefore, only the cost of rehabilitation activities is considered to incorporate solely the additional agency cost caused by platooning. Rehabilitation activities are applied when a pavement reaches its service life (n_s), where the accumulated damage within the pavement exceeds the predefined serviceability limit(s). The serviceability limit(s) can be defined in terms of accumulated IRI, rutting, or fatigue cracking, which are calculated by the previously introduced pavement design approach. The rehabilitation activity considered in this study is resurfacing where a certain amount of pavement is removed from the surface and an asphalt overlay is placed. Son and Al-Qadi (2014) reported that right after rehabilitation, the pavement condition could be recovered up to 80–100%. Herein, for analysis simplicity, initial IRI is assumed to be fully (100%) recovered after rehabilitation activity is applied.

The user cost in pavement life cycle cost refers to additional cost to the public due to travelling on rough pavement with various distresses. The user costs are generally reported as function of IRI. The equation developed by Ziyadi et al. (2018) is used to compute the additional energy consumption due to pavement roughness. Figure 31 computes the energy consumption as a function of other variables (e.g., speed) as well as IRI. To isolate the effect of IRI, this equation should be executed twice with initial IRI_0 (initial IRI) and IRI_t (IRI at time t). The difference between these two executions gives the additional energy consumption due to IRI. This resultant energy can be converted to cost by multiplying it with diesel liter required per unit energy (DLR) and the cost of one-liter diesel (CLD) (Figure 32).

$$E = \frac{p}{v} + (k_\alpha IRI + d_\alpha) + bv + (k_c IRI + d_c)v^2$$

Figure 31. Equation. Energy consumption.

where

E = estimated energy consumption per mile (kj/mile);
v = speed (mph); and

k_α, k_c, d_c, d_α b, and p = model coefficients which are given as 1.4, 1.36 x 10^{-4},2.39, 1.9225 x 10^4, -2.6435 x 10^2, 8.2782 x 10^4 for large trucks.

$$TEC = \Delta E * \text{diesel liter required} * \text{ the cost of one} - \text{liter diesel}$$

Figure 32. Equation. Total energy cost.

where TEC = total energy cost.

Figure 33 presents the objective function of the optimization model. The first and second parts correspond to the agency cost and user cost due to pavement roughness, respectively. The third part is the fuel cost due to reduced aerodynamic drag. This study aims to minimize the summation of these costs by optimizing the trade-off between pavement LCC and the fuel cost due to aerodynamic drag.

This optimization model has two constraints. The first constraint determines how much a truck can be shifted within a lane, which is the function of both vehicle width and lane width (Figure 34). The second constraint defines the boundaries of inter-vehicle spacing, which were set using engineering intuition because there is no formal regulation (Figure 35). The lower bound was set as 3 m; this is the lowest reported inter-vehicle spacing used in testing truck platooning (Browand et al., 2004). The upper bound was selected as 60 m; it is the minimum following distance for human-driven trucks.

$$\min_{\bar{z},s} \left(\sum_{i=1}^{\left| \left\lfloor \frac{A_p}{n_s(\bar{z},s)} \right\rfloor \right|} C \frac{1}{(1+r)^{n_s(\bar{z},s)*i}} + \sum_{k=1}^{A_p} U_c(IRI(\bar{z},s)_k) \frac{1}{(1+r)^k} + \sum_{k=1}^{A_p} UCA_k \frac{1}{(1+r)^k} \right)$$

Figure 33. Equation. Objective function.

subject to

$$-\frac{L_w - V_w}{2} \leq z_i \leq \frac{L_w - V_w}{2}$$

Figure 34. Equation. Constraint for lateral offset.

$$3\,m \leq s \leq 60\,m$$

Figure 35. Equation. Constraint for inter-vehicle separation.

where

z = 1xN vector that is the lateral position of each truck in a N-sized platoon;
L_w = lane width;
V_w = vehicle width;
s = inter-vehicle spacing between trucks in a platoon;

C = cost of a rehabilitation activity;

A_p = analysis period;

r = discount rate;

$n_s(\bar{z}, s)$ = service life a pavement; and

$U_c(IRI(\bar{z})_k)$ = user cost due to the pavement roughness that are computed using Equation 7.

To solve Figure 33, three evolutionary optimization algorithms from the MATLAB optimization toolbox were used: pattern-search algorithm (PS), genetic algorithm (GA), and particle-swarm optimization (SW). These algorithms start with generating a set of candidate solutions that evolve to the optimum points at each iteration. Each algorithm has its own technique for defining evaluation of the candidate points. While GA mimics the evaluation of animals, SW emulates the swarm intelligence for finding optimum points. PS is a derivative-free direct-search method that converges to the solution using the theory of positive bases. The details about each algorithm is given in MATLAB (2019).

CASE STUDY

Pavement-Design Parameters

The optimization model was evaluated on pavement that is demonstrated in Figure 36. In this study, the platoons are assumed to be formed by FHWA classification class 9 vehicles, because they were found to be the most common truck type (70%) based on 2016 weigh-in-motion (WIM) data collected at Frackur, Illinois. Using the same data, a typical axle configuration was extracted for class 9 trucks whose gross weight is 36.3 tons, which is the legal limit in the United States (Figure 37). Annual average daily truck traffic is assumed to be 8,000 for the simulated pavement section.

Material parameters for both AC was obtained from the Long-Term Pavement Performance database. The material properties are given in Gungor and Al-Qadi (2020). Strong material parameters were considered in this study. This is an appropriate pavement design for the considered simulated annual average daily truck traffic. The other pavement design-related parameters that were assumed in this study are given in Table 1.

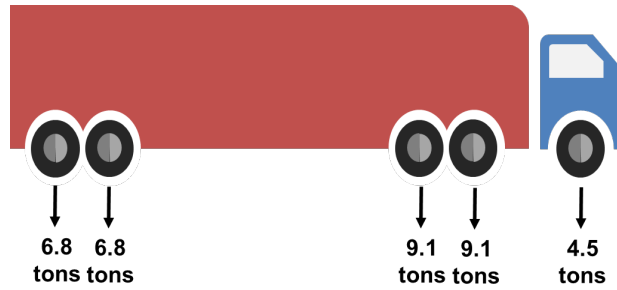**Figure 36. Photo. Pavement cross section.**

Figure 37. Photo. Simulated class 9 truck.

Table 1. Assumed Pavement Design Parameters

Variable name	Value	Variable name	Value
Initial IRI	0.95 m/km	Percent plasticity index of the soil	4 %
AC temperature	22.2 C	Percent air voids	4 %
Lane width	3.6 m	Resilient modulus of base	275 MPa
Axle width	2.4 m	Resilient modulus of subgrade	35 MPa
Average annual precipitation	995.7 mm	Groundwater table depth	3 m
Freezing Index	50 %	Effective asphalt content by volume	4.6 %
Percent passing the 0.02-mm sieve	2 %	Percent passing the 0.075-mm sieve	7 %

PAVEMENT LIFE CYCLE COST ANALYSIS

This study followed the pavement life cycle cost analysis (LCCA) guidelines published by the Illinois Department of Transportation (IDOT). These guidelines suggest an analysis period (A_p) as 45 years and discount rate as 3%. Additionally, the triggering value for pavement rehabilitation is assumed to be 2.5 m/km of IRI or 6.5 mm of rutting. The year when the roughness or rutting reach these values was considered the pavement's service life. The type of rehabilitation considered is a 5 cm overlay; and it was assumed that, after each rehabilitation, the pavement exhibits the same performance as previously. The cost for this overlay was computed as $15.7 x 10^4$ \$/km-lane from the IDOT guidelines, assuming a 3.6 m lane width. Future work is required to define the optimized triggering time for rehabilitation, as used by Bai et al. (2015), to minimize pavement's overall LCCA when platooning is considered.

Table 2. Assumed Values for Algorithm Parameters

GA		PSO		PSA	
ConstraintTolerance	1.00E-03	FunctionTolerance	1.00E-06	FunctionTolerance	1.00E-06
CrossoverFraction	0.8	InertiaRange	[0.1,1]	InitialMeshSize	1
FunctionTolerance	1.00E-06	MaxGenerations	100 * # of Variables	MaxGenerations	100 * # of Variables
MaxGenerations	100 * # of Variables	SelfAdjustmentWeight	1.49	MeshContractionFactor	0.5
MutationFcn	'mutationgaussian'	SocialAdjustmentWeight	1.49	MeshExpansionFactor	2
PopulationSize	15 * # of Variables	SwarmSize	15 * # of Variables	MeshTolerance	1.00E-06

Optimization Algorithm Comparisons

The evolutionary optimization algorithms used in this study have a set of parameters that impact the performance of the algorithms. The objective function given in Figure 33 was solved by three evolutionary algorithms: GA, PS, and SW. Assumed values for important parameter for each algorithm are listed in Table 2. Varying platooning sizes ranging from two to 10 trucks were considered. The results are presented in Figure 38. The y-axis represents the net gain, which is the difference between the base-case scenario and optimized scenario. The base-case scenario simulates the platooning application where the trucks are perfectly aligned (i.e., there is no lateral shift) with minimum spacing (i.e., 3 m). Because these three algorithms have stochastic parts, they were run five times for each number of trucks in a platoon. Each point in Figure 38-A, Figure-38-B, and Figure-38-C represent the results from each run. As seen, GA and PS generally have greater variance in results as compared to SW. GA and PS have comparable results in general as seen from Figure 38-D. However, SW consistently outperformed both GA and PS algorithms by producing higher net gain for all platoon sizes.
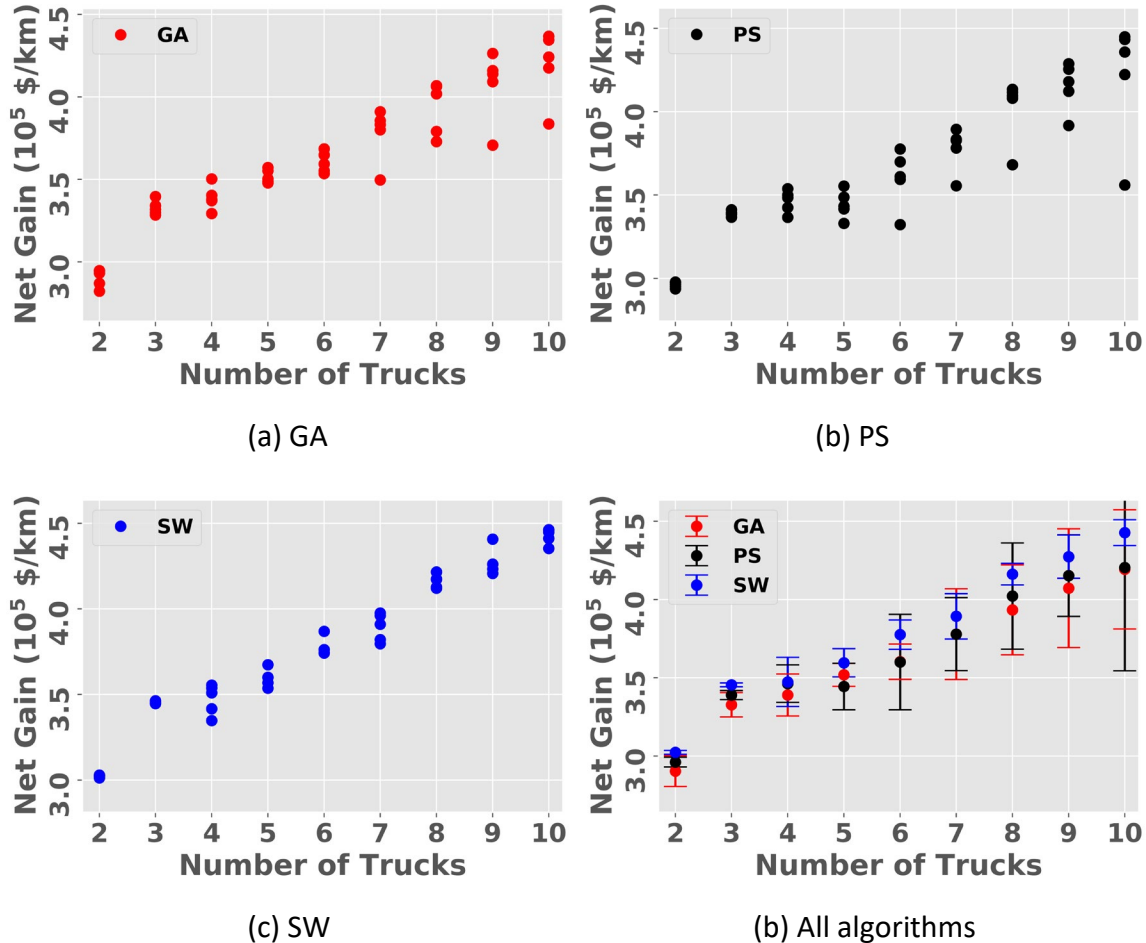

(a) GA

(b) PS

(c) SW

(b) All algorithms

Figure 38. Chart. Optimization results of each algorithm.

Optimum Platoon Skeletons and Corresponding Costs

This section presents the optimum platoon skeletons and corresponding cost distribution obtained from the SW algorithm. Figure 39 shows the optimized truck configuration for a platoon size of 10. The optimum spacing between trucks was found to be 3.3 m, which is very close to the minimum boundary. This is because the governing failure mode in this case was rutting in base layer and subgrade (not AC), which is not affected by the change in spacing because both materials are linear elastic.
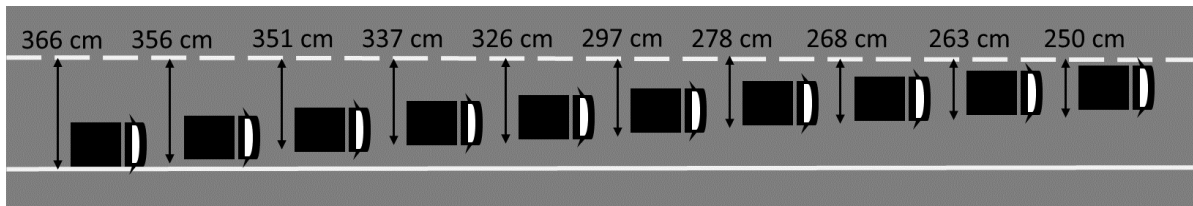

Figure 39. Photo. Optimum skeleton for the platoon with 10 trucks.

The optimized lateral position of trucks for other platoon sizes are given in Table 3 along with resultant inter-vehicle distances. Trucks are placed in a staggered pattern that can be investigated to develop more efficient solutions for the optimization problem instead of using evolutionary algorithms. Also, inter-vehicle distance was found to be close to the minimum bound, as explained previously.

Table 3. Optimum Skeletons for Varying Platoon Sizes

# of truck	P1 (cm)	P2 (cm)	P3 (cm)	P4 (cm)	P5 (cm)	P6 (cm)	P7 (cm)	P8 (cm)	P9 (cm)	P10 (cm)	Sep. (cm)
2	361	342									402
3	338	352	366								389
4	354	366	345	333							425
5	244	263	271	279	298						408
6	351	333	314	297	278	259					344
7	360	343	325	307	289	270	253				331
8	247	251	270	279	308	331	339	351			332
9	244	260	268	283	298	321	337	352	358		317
10	366	356	351	337	326	297	278	268	263	250	330

The cost-distribution results that correspond to the platooning skeletons are given in Table 4. These costs should be interpreted as follows: assuming 100% ACT penetration and all ACTs travel in determined optimum configuration for each size. These costs represent resultant agency and user costs in the analysis period of 45 years.

As seen for all cases, net gain for agency cost is positive and net gain for user cost is negative. While lateral shift of the truck decreases pavement damage accumulation and agency cost, it also increases aerodynamic drag on each truck, increasing user cost. Total net gain increases with increasing platoon size, as demonstrated in Figure 39. Agency cost for the base scenario is the same because trucks travel with no lateral shift for all platoon sizes.

Table 4. Optimization Results for Varying Platoon Sizes

# of truck	Base Scenario ($M/km)			Optimized Scenario ($M/km)			Net Gain ($M/km)		
	Agency Cost	User Cost	Total Cost	Agency Cost	User Cost	Total Cost	Agency Cost	User Cost	Total Cost
2	0.94	4.27	5.21	0.5	4.41	4.91	0.44	-0.14	0.3
3	0.94	4.07	5.01	0.45	4.19	4.64	0.49	-0.12	0.37
4	0.94	3.9	4.84	0.4	4.06	4.45	0.54	-0.16	0.38
5	0.94	3.79	4.73	0.4	3.94	4.34	0.54	-0.15	0.39
6	0.94	3.71	4.66	0.35	3.88	4.23	0.59	-0.16	0.43
7	0.94	3.66	4.6	0.33	3.82	4.16	0.61	-0.16	0.45
8	0.94	3.62	4.57	0.3	3.79	4.08	0.64	-0.16	0.48
9	0.94	3.59	4.54	0.3	3.73	4.02	0.64	-0.13	0.51
10	0.94	3.57	4.51	0.28	3.71	3.99	0.66	-0.14	0.52

Over an analysis period of 45 years of a selected pavement design, the proposed optimized lateral position of trucks in the platoon reduces the relative total cost by 9%. These cost savings may change for various pavement sections, ACT penetration rates, climates, and traffic conditions. However, the net gain is expected to increase as the size of the platooning increases. The platooning size may be better optimized when considering lane management and network analysis. Additionally, dynamic programming should be considered to reduce computational time. Further analysis is needed to consider the shifting of platoon groups rather than single trucks.

CHAPTER 5: CONCLUSION

One of the expected changes associated with the introduction of autonomous and connected trucks is the formation of truck platoons, which may decrease fuel consumption, improve traffic flow, and increase highway safety. However, truck platoons are also expected to increase the damage accumulation rate within pavement because of channelized load application (i.e., constant lateral position of the trucks) and reduced resting time (i.e., time between two consecutive loading). This report proposed a control strategy that leverages auto-pilot technology existing in ACTs by optimizing the lateral position and inter-vehicle spacing of trucks in a platoon to reduce pavement damage while preserving fuel efficiency. The proposed strategy has been evaluated on a pavement case study. The relative total costs to agencies and users may be reduced by 9%. A holistic evaluation of the presented approach, considering various pavement sections, climates, traffic levels, and ACT penetration rates, need to be investigated.

REFERENCES

Alam, A., B. Besselink, V. Turri, J. Martensson, & K. H. Johansson. (2015). Heavy-duty vehicle platooning for sustainable freight transportation: A cooperative method to enhance safety and efficiency. *IEEE Control Systems*, *35*(6), 34–56.

Ansys, A. F. (2011). 14.0 theory guide. ANSYS inc, 390, 1.

Al-Qadi, I. L., J. A. Hernandez, A. Gamez, M. Ziyadi, O. E. Gungor, & S. Kang. (2015). Impact of wide-base tires on pavements: A national study. *Transportation Research Record* 0361198118757969.

Al-Qadi, I. L., & H. Wang. (2012). Impact of wide-base tires on pavements: Results from instrumentation measurements and modeling analysis. *Transportation Research Record*, *2304*(1), 169-176.

Bai, Y., O. E. Gungor, J. A. Hernandez-Urrea, Y. Ouyang, & I. L. Al-Qadi. (2015). Optimal pavement design and rehabilitation planning using a mechanistic-empirical approach. *EURO Journal on Transportation and Logistics*, *4*(1), 57–73.

Bonnet, C., & H. Fritz. (2000). *Fuel consumption reduction in a platoon: Experimental results with two electronically coupled trucks at close spacing* (No. 2000-01-3056). SAE Technical Papers.

Browand, F., J. McArthur, & C. Radovich. (2004). *Fuel saving achieved in the field test of two tandem trucks* (Technical Report UCB-ITS-PRR-2004-20). California PATH Program, Institute of Transportation Studies, University of California, Berkeley.

Castillo, D., & I. Al-Qadi. (2018). Importance of heterogeneity in asphalt pavement modeling. *Journal of Engineering Mechanics*, *144*(8), 04018060.

Eilers, S., J. Mårtensson, H. Pettersson, M. Pillado, D. Gallegos, M. Tobar, & M. Adolfson. (2015). COMPANION—Towards co-operative platoon management of heavy-duty vehicles. In *2015 IEEE 18th International Conference on Intelligent Transportation Systems (ITSC)*, 1267–73.

Elseifi, M. A., I. L. Al-Qadi, & P. Jun Yoo. (2006). Viscoelastic modeling and field validation of flexible pavements. *Journal of Engineering Mechanics*, *132*(2), 172–78.

Federal Highway Administration (FHWA) (2004). *Federal size regulations for commercial motor vehicles*.

Gaudet, B. (2014). *Review of cooperative truck platooning systems.* National Research Council Canada.

Gungor, O. E., I. L. Al-Qadi, A. Gamez, & J. A. Hernandez. (2016a). In-situ validation of three-dimensional pavement finite element models. In *The Roles of Accelerated Pavement Testing in Pavement Sustainability*, 145–159. Springer.

Gungor, O. E., J. A. Hernandez, A. Gamez, & I. L. Al-Qadi. (2016b). Quantitative assessment of the effect of wide-base tires on pavement response by finite element analysis. *Transportation Research Record: Journal of the Transportation Research Board 2590*, 37–43.

Gungor, O. E., I. L. Al-Qadi, A. Gamez, & J. A. Hernandez. (2017). Development of adjustment factors for MEPDG pavement responses utilizing finite-element analysis. *Journal of Transportation*

Engineering, Part A: Systems, *143*(7), 04017022.

Gungor, O. E., & I. L. Al-Qadi. (2020). All for one: Centralized optimization of truck platoons to improve roadway infrastructure sustainability. *Transportation Research Part C: Emerging Technologies*, *114*, 84–98.

Hernandez, J. A., & I. L. Al-Qadi. (2016). Semicoupled modeling of interaction between deformable tires and pavements. *Journal of Transportation Engineering, Part A: Systems*, *143*(4), 04016015.

Hinterberger, C., M. Garcia-Villalba, & W. Rodi. (2004). Large eddy simulation of flow around the Ahmed body. In *The aerodynamics of heavy vehicles: Trucks, buses, and trains*, 77–87. Springer.

Humphreys, H. (2017). A computational fluid dynamics analysis of a driver-assistive truck platooning system with lateral offset. Master's thesis, Auburn University.

Humphreys, H. L., J. Batterson, D. Bevly, & R. Schubert. (2016). *An evaluation of the fuel economy benefits of a driver assistive truck platooning prototype using simulation* (No. 2016-01-0167). SAE Technical Papers.

International Energy Agency (IEA). (2017). *The future of trucks implications for energy and environment*, Technical Report.

Jacob, B., & O. Arbeit de Chalendar. (n.d.). Truck platooning: Expected benefits and implementation conditions on highways. *Heavy Vehicle Transportant Technology (HVTT) International Symposium*.

Lammert, M. P., A. Duran, J. Diez, K. Burton, & A. Nicholson. (2014). Effect of platooning on fuel consumption of class 8 vehicles over a range of speeds, following distances, and mass. *SAE International Journal of Commercial Vehicles*, *7*, 626–39.

Lanfrit, M. (2005). A best practice guideline to handle automotive external aerodynamics with FLUENT. *Fluent, Inc., Technical Notes*.

Liu, Y., & A. Moser. (2003). Numerical modeling of airflow over the Ahmed body. *Proceedings of CFD, Canada*, 507–512.

Lu, X. Y., & S. E. Shladover. (2011). *Automated truck platoon control*. Report to Federal Highway Administration under Cooperative Agreement DTFH61-07-H-00038.

National Cooperative Highway Research Program (NCRP). (2004). *Guide for mechanistic–emprical design of new and rehabilitated pavement structures*.

Robinson, T., E. Chan, & E. Coelingh. (2010). Operating platoons on public motorways: An introduction to the sartre platooning programme. In *17th World Congress on Intelligent Transport Systems 1*, 12.

Smith, A. F., C. M. Horrell, J. J. Grossmann, J. R. Feldman, & A. R. Bruccoleri. (2012). *U.S. Patent No. 8,100,461*. Washington, DC: U.S. Patent and Trademark Office.

Son, S., & I. L. Al-Qadi. (2014). Engineering cost-benefit analysis of thin, durable asphalt overlays. *Transportation Research Record 2456*(1), 135–145.

Spalart, P. R. (1997). Comments on the feasibility of LES for wings, and on a hybrid RANS/LES approach. In *Proceedings of First AFOSR International Conference on DNS/LES*. Greyden Press.

Suzuki, Y. (2011). A new truck-routing approach for reducing fuel consumption and pollutants emission. *Transportation Research Part D: Transport and Environment 16*(1), 73–77.

Tsugawa, S. (2014). Results and issues of an automated truck platoon within the energy ITS project. In *2014 IEEE Intelligent Vehicles Symposium Proceedings,* 642–47.

Tsugawa, S., S. Jeschke, & S. E. Shladover. (2016). A review of truck platooning projects for energy savings. *IEEE Trans. Intelligent Vehicles 1*(1), 68–77.

Tsugawa, S., S. Kato, & K. Aoki. (2011). An automated truck platoon for energy saving. In *2011 IEEE/RSJ International Conference on Intelligent Robots and Systems (IROS)*, 4109–14. IEEE.

Van Leeuwen, P. M. (2009). Computational analysis of base drag reduction using active flow control. Master's thesis, Delft University of Technology.

Wang, H., & I. L. Al-Qadi. (2010). Impact quantification of wide-base tire loading on secondary road flexible pavements. *Journal of Transportation Engineering*, *137*(9), 630–39.

Yoo, P. J., & I. L. Al-Qadi. (2007). Effect of transient dynamic loading on flexible pavements. *Transportation Research Record*, *1990*(1), 129–40.

Zabat, M., N. Stabile, S. Farascaroli, & F. Browand. (1995). *The aerodynamic performance of platoons: A final report*. California Partners for Advanced Transit and Highways.

Ziyadi, M., H. Ozer, S. Kang, & I. L. Al-Qadi. (2018). Vehicle energy consumption and an environmental impact calculation model for the transportation infrastructure systems. *Journal of Cleaner Production*, *174*, 424–436.